PCCP

Spectroscopic and chemical characterization of active and inactive Cu species in NO decomposition catalysts based on Cu-ZSM5

Patrick Da Costa,†[a] Björn Modén,[a] George D. Meitzner,[b] Deuk Ki Lee‡[a] and Enrique Iglesia*[a]

[a] *Department of Chemical Engineering, University of California at Berkeley, Berkeley CA 94720, USA. E-mail: iglesia@cchem.berkeley.edu*
[b] *Edge Analytical, Inc., El Paso TX 79912, USA*

Received 16th April 2002, Accepted 26th June 2002
First published as an Advance Article on the web 8th August 2002

The number and type of Cu^{2+} species present on O_2-treated Cu-ZSM5 catalysts (Si/Al = 13.1–14.6) with varying Cu/Al ratios (0.12–0.60) were measured using temperature-programmed reduction in H_2 or CO and desorption of O_2 with He as the carrier. The effluent stream was monitored using mass spectrometry and the structure and oxidation state was determined in parallel by X-ray absorption spectroscopy. Isolated Cu^{2+} monomers and oxygen-bridged Cu^{2+} dimers interacting with Al–Al next nearest neighbor pairs were the predominant Cu species on these catalysts. The fraction of Cu present as dimers increased from 0.46 to 0.78 as Cu/Al ratios increased from 0.12 to 0.60, as expected from the decreasing average Cu–Cu distance with increasing Cu content. In contrast, monomers reached a plateau of ~0.15 Cu^{2+}/Al, suggesting that only some Al–Al pairs can interact with small Cu^{2+} monomer structures, while a much larger fraction can bind with larger oxygen-bridged Cu^{2+} dimers. The measured distribution of Cu dimers and monomers is consistent with the number and bond distances of Al–Al pairs for the Si/Al ratio in these ZSM5 samples. The distributions of Cu species obtained from the amount of CO_2 formed (from CO), the amount of H_2O formed (from H_2), and the amount of CO adsorbed after reduction in CO are in excellent agreement. The number of oxygen atoms removed as O_2 was significantly smaller than that removed with H_2 or CO, suggesting that only proximate Cu dimers autoreduce *via* recombinative desorption steps. NO decomposition turnover rates (normalized per Cu dimer) were nearly independent of Cu content, except at the lowest Cu/Al ratio, consistent with the involvement of Cu dimers as the active Cu species in NO decomposition redox cycles on Cu-ZSM5. Multiple O_2 and CO_2 peaks during desorption and reduction in CO suggest the presence of Cu dimers with varying oxygen binding energy and reactivity. The Cu dimers initially formed at low Cu/Al contents during exchange are less reducible, consistent with their lower NO decomposition turnover rates.

Introduction

Direct decomposition of NO to N_2 and O_2 remains the most robust strategy for NO_x removal from combustion streams, because it does not require a co-reactant. NO decomposition is thermodynamically favored and Cu-ZSM5[1] and supported noble metals[2,3] catalyze this reaction, albeit at impractically low rates. NO decomposition pathways and the sites required for this reaction are relatively well understood for noble metal catalysts. Many studies of the active structures and NO decomposition pathways have been conducted on Cu-ZSM5 and other cation-exchanged zeolites. The number and catalytic role of the various exchanged Cu cations and CuO species and the details of N–N and O–O bond formation during NO decomposition, however, remain subjects of active debate.

The exchange of Cu ions onto ZSM5 using aqueous Cu salts leads to Cu^{2+} species. Some of these species autoreduce to Cu^{+} during thermal treatment in He with the concurrent desorption of extraframework oxygen atoms as O_2.[4–7] The expected presence of such species, together with electron spin resonance and thermogravimetric studies,[7] suggest that redox cycles are responsible for NO decomposition turnovers. Infrared spectra of adsorbed CO and NO provided indirect evidence for the reversible cycling between Cu^{2+} and Cu^{+} during switching between O_2 and He streams at 773 K.[8] These cycles were confirmed by X-ray photoelectron (XPS) and X-ray absorption (XAS) spectroscopic studies.[9] The parallel increase in the concentration of Cu^{+} species detected by XAS and in the rate of NO decomposition was used as evidence for Cu^{+} as a reaction intermediate.[10,11] A mechanism involving NO coordination to Cu^{2+} without the involvement of reduction-oxidation cycles has also been suggested[12] but it has not been supported by experimental evidence. N–N formation has been proposed to occur *via* adsorption of two NO molecules on a single Cu^{+} site to form dinitrosyl complexes $\{Cu^{+}(NO)_2\}$, which decompose to N_2O and $Cu^{2+}O^{-}$.[6,13,14] The awkward charge balance associated with $Cu^{2+}O^{-}$ species[15–17] can be avoided by placing each of the two NO molecules in the two vicinal Cu^{+} cations within a $\{Cu^{+}$–□–$Cu^{+}\}$ pair (□; oxygen vacancy), which would then form N_2O and an oxygen-bridged copper dimer $\{Cu^{2+}$–O^{2-}–$Cu^{2+}\}^{2+}$.[4,18–20] This step resolves the charge balance concerns and it is consistent with the observed increase in NO decomposition turnover rates as the Cu/Al ratio increases and oxygen-bridged dimers become more prevalent.[21]

Oxidized Cu dimers $\{Cu^{2+}$–O^{2-}–$Cu^{2+}\}^{2+}$ and their reduced forms $\{Cu^{+}$–□–$Cu^{+}\}^{2+}$ are not the only Cu species that can co-exist in Cu-ZSM5, as shown by temperature-programmed

† Current address: Laboratoire Reactivite de surface, UMR CNRS 7609, Tour 54-55 case 178, Universite Pierre et Marie Curie, 4, place Jussieu, 75252 Paris Cedex 05, France.
‡ Current address: Division of Civil and Environmental Engineering, Kwangju University, Kwangju, 503-703 Korea.

 DOI: 10.1039/b203700a

reduction studies using H_2 or CO as reductants.[18,20] These studies have detected CuO, isolated Cu^{2+}, as well as Cu dimers $\{Cu^{2+}–O^{2-}–Cu^{2+}\}^{2+}$. A quantitative assessment of the Cu^{2+}/Cu^{+} speciation during catalyst synthesis, thermal treatment, and catalytic NO decomposition has remained elusive, because of the dispersed nature of these structures, the non-uniform nature of the samples, and the dearth of available techniques to assess their structural features at realistic conditions. Yet, such site speciation remains the essential requirement to establish conclusively the redox nature and the site requirements of NO decomposition pathways. This challenge can be addressed most effectively by applying complementary spectroscopic and chemical techniques able to measure concentrations for each Cu species, so that their respective abundances can be related to the rate of the catalytic reaction of interest, in this case NO decomposition.

Elsewhere, we have reported transient and steady-state kinetic studies that provide mechanistic evidence for the involvement of Cu^{2+} dimers with one bridging extraframework oxygen atom as the prevalent state of the active Cu sites involved in NO decomposition and in O–O bond formation.[22,23] Here, we report chemical and spectroscopic characterization data for a series of Cu-ZSM5 samples with varying Cu/Al ratio using X-ray absorption spectra during oxygen removal by treatment with H_2, CO, or He, along with mass spectrometric analysis of the amount of oxygen removed during these thermal treatments (as H_2O, CO_2, or O_2). These combined methods have led to a quantitative assessment of the number of Cu^{2+} and $\{Cu^{2+}–O^{2-}–Cu^{2+}\}^{2+}$ species for samples with a wide range of Cu/Al ratios and to the definite correlation of catalytic NO decomposition rates with the number of Cu dimers present in each sample.

Experimental methods

Catalyst synthesis

Cu-ZSM5 catalysts were prepared with different Cu/Al ratios by ion exchange using an aqueous solution of $Cu(CH_3COO)_2{\cdot}H_2O$ (Sigma Aldrich, ACS reagent) and Na-ZSM5 (Zeochem; two batches, Si/Al = 13.2, 14.5). The molarity of this solution (100 cm^3/g-ZSM5) was varied between 0.01 and 0.1 M $Cu(CH_3COO)_2{\cdot}H_2O$ in order to obtain Cu/Al ratios between 0.12 and 0.60. The pH of the solution was 5.5–6.0 during exchange. The exchange was carried out at ambient temperature for 20 h and the samples were then rinsed six times with doubly de-ionized water (30 cm^3 (g ZSM5)$^{-1}$ each time) with an intervening filtering step between each rinse. These rinse cycles were carried out in order to ensure that intraparticle liquids did not contain Cu cations, which would form crystalline CuO species during drying and thermal treatment. For some of the samples, this exchange procedure was repeated two or three times in an attempt to increase the Cu/Al ratio. Samples were then dried in static ambient air at 383 K for 24 h and pelleted and sieved in order to retain agglomerates with 125–250 μm diameter. The Si, Al, Na and Cu contents were measured by ion-coupled plasma emission spectroscopy or atomic absorption (Galbraith Laboratories) and reported in Table 1. We refer to samples as Cu(x), where x is the atomic Cu/Al ratio for each sample.

Table 1 Catalyst composition. Cu(0.38) and Cu(0.58) are from one ZSM5 batch, and Cu(0.12), Cu(0.36) and Cu(0.60) are from another batch

Catalyst	Cu(0.12)[a]	Cu(0.36)	Cu(0.38)	Cu(0.58)	Cu(0.60)
Cu (wt.%)	0.76	2.25	2.24	3.31	3.88
Si (wt.%)	38.2	36.3	37.9	36.0	37.5
Al (wt.%)	2.76	2.66	2.50	2.42	2.73
Na (wt.%)	1.69	0.64	0.51	<0.08	<0.11
Si/Al	13.3	13.1	14.6	14.3	13.2

[a] Molar ratio of Cu to total Al.

Kinetics of oxygen removal and Cu reduction in H_2, CO and He

The consumption of H_2 and the formation of H_2O were monitored as a function of temperature during reduction in H_2 (H_2-TPR). The formation of CO_2 during reduction in CO (CO-TPR) and the desorption of O_2 during temperature ramping using He as the carrier gas (TPD) were also measured on all samples. Catalyst samples (0.2–0.3 g) were held within a quartz tube and the effluent was analyzed using mass spectrometry as the sample temperature was increased in flowing H_2, CO, or He. Mass signals for H_2 (2 amu), He (4 amu), H_2O (18 amu), CO (28 amu), O_2 (32 amu), Ar (40 amu) and CO_2 (44 amu) were monitored every 10 s using a mass spectrometer (MKS Instruments, Orion Compact Residual Gas Analyzer) equipped with a differentially pumped atmospheric sampling system. CO_2 and H_2O response factors were calculated by reducing known amounts of CuO to Cu in CO and H_2, respectively, and measuring the amount of CO_2 and H_2O formed.

Samples were treated similarly before H_2-TPR, CO-TPR and O_2-TPD measurements. The samples were contacted with a flow of 50% O_2/He (Matheson) (4.165 cm^3 s^{-1} g^{-1}; denoted herein as O_2 gas) as the sample temperature was increased from ambient to 773 K at 0.167 K s^{-1} and held at 773 K for 2 h. The samples were then cooled to ambient temperature and the O_2 gas was replaced with He (8.335 cm^3 s^{-1} g^{-1}) in order to remove any physisorbed species. For H_2-TPR, the quartz tube was then cooled down to ~220 K using liquid nitrogen, and He was replaced with 5% H_2/Ar (Praxair) at 2.085 cm^3 s^{-1} g^{-1}. After the intensity at 2 amu reached a constant value, the sample temperature was increased to 923 K at 0.167 K s^{-1}. For CO-TPR, He was replaced with 1% CO/He (Praxair) at 2.085 cm^3 s^{-1} g^{-1} and the samples were heated to 700 K at 0.167 K s^{-1}. A H_2-TPR was also carried out after a CO-TPR by cooling the sample to ambient temperature, then replacing the 1% CO/He gas with He in order to remove weakly adsorbed CO, and finally replacing He with 5% H_2/Ar. Then, the H_2-TPR procedure described above was repeated, but with a final temperature of 800 K instead of 923 K. For O_2 TPD, the He flow rate was decreased to 2.5 cm^3 s^{-1} g^{-1} and the sample was heated to 1000 K at 0.167 K s^{-1}. Throughout the manuscript, when O/Cu ratios are reported, the Cu refers to the total number of Cu atoms in the sample. When O/Cu_{dimer} is reported instead, it refers to the total number of Cu atoms present in dimers.

In situ X-ray absorption spectroscopy (XAS) experiments

X-ray absorption spectra were measured using beamline 4-1 at the Stanford Synchrotron Radiation Laboratory. The ring was operated at 30–100 mA and 3.0 GeV during the experiments. A two-crystal Si(220) monochromator was detuned by 30% in order to minimize harmonics. Our beam definition slit had vertical and horizontal apertures of 0.2 and 15 mm, respectively, which defined a maximum energy resolution of 1 eV at the Cu K edge (8979 eV). The intensities of the incident beam (I_0), of the beam after passing through the sample (I_1), and of the beam after passing through a 7.5 μm Cu foil placed after the sample (I_2) were monitored using N_2-filled ion chamber detectors. Dynamic spectra were acquired during transient measurements at 11.25 eV increments from 8880 to 8970 eV, 0.6 eV increments from 8970 to 9005 eV, and 8 eV increments from 9005 to 9223 eV. The absorption intensity data were integrated

for 0.5 s at each energy for a total acquisition time of 144 s per transient spectrum.

Samples (10 mg) were held within a quartz capillary (0.8 mm inner diameter, 0.1 mm wall thickness), which acts as an isothermal tubular reactor with plug-flow hydrodynamics and walls transparent to X-rays.[24,25] The samples were contacted with a flow of 50% O_2/He (Matheson) (3.33 $cm^3\ s^{-1}\ g^{-1}$) as the temperature was increased from ambient to 773 K at 0.167 K s^{-1} and held at 773 K for 2 h. The samples were then cooled to ambient temperature and the O_2-containing stream was replaced by He (3.33 $cm^3\ s^{-1}\ g^{-1}$) in order to remove any physisorbed species, as described above. Finally, H_2-TPR experiments were performed by replacing the He with 5% H_2/Ar (Praxair) at 3.33 $cm^3\ s^{-1}\ g^{-1}$, and increasing the sample temperature to 800 K at 0.067 K s^{-1}. The heating rate was kept at these low values in order to obtain essentially isothermal conditions during each XANES spectrum.

X-Ray absorption near-edge (XANES) analysis

Near-edge and fine structure data analyses were carried out using WinXAS version 2.1.[26,27] The energy scale was calibrated by assigning the first inflection point in the Cu foil standard to an energy of 8979 eV. A linear regression fit to the pre-edge region between 8891 and 8952 eV was subtracted from the spectrum, and the spectrum was normalized using a second-order polynomial fit of the post-edge region (9068–9223 eV). Principal component analyses (PCA)[28] and linear combination[29] methods were used in order to measure the number, type, and concentration of each structurally distinct Cu species contributing to the 8900–9100 eV energy region in each spectrum.

Catalytic NO decomposition rate measurements

Catalytic NO decomposition rates were measured using a compact multi-tube (2.5 mm inner diameter) reactor designed to evaluate eight samples (50 mg) simultaneously at a given temperature and feed composition and at individually controlled reactant flow rates. The reactors were tightly held within a cylindrical steel block inside a resistively heated furnace (Applied Test Systems, Series 3210, 1290 W). Thermocouples were placed within the steel block a short distance from each reactor near the middle of each catalyst bed. Catalyst samples were treated in He (UHP grade; 0.50 $cm^3\ s^{-1}$) for 1 h at 823 K before introducing a reactant mixture containing 1.0% NO/9.98% Ar/89.02% He and denoted here as 1% NO gas (Matheson). The flow of the reactant mixture was kept at 1.0 $cm^3\ s^{-1}$ through each reactor using fine metering valves. The effluent streams from each reactor were sequentially routed to the mass spectrometer for analysis using an eight-port switching valve (Valco Instruments, Multiposition valve STF). The species monitored by mass spectrometry were: He (4 amu), NO (30 amu), N_2 (28 amu), O_2 (32 amu), Ar (40 amu), N_2O (44 amu), and NO_2 (46 amu). The mass spectrometer response was calibrated before and after each experiment using two certified gas mixtures containing 0.05% N_2, 0.05% O_2, 0.05% N_2O, 10% Ar, and 89.85% He, and 0.05% NO_2, 9.94% Ar, and 90.01% He, both provided by Praxair.

Results and discussion

Cu speciation in Cu-ZSM5 after exchange and thermal treatment

Several types of Cu species can co-exist after synthesis and thermal treatment in air (Fig. 1). During synthesis *via* ion-exchange, Cu^{2+} species in aqueous acetate solutions can replace Na^+ cations as solvated $\{Cu^{2+}–(OH)^-\}^+$ ions,[30] which can then react with zeolitic OH groups or with another

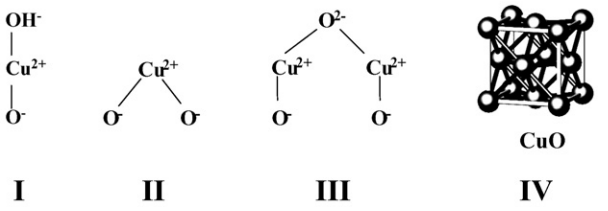

Fig. 1 Divalent Cu species in Cu–ZSM5: (I and II): isolated copper species, (III): copper dimer species, (IV): bulk copper oxide.

$\{Cu^{2+}–(OH)^-\}^+$ ion during subsequent thermal treatment to form Cu^{2+} monomers or $\{Cu^{2+}–O^{2-}–Cu^{2+}\}^{2+}$ dimers, respectively, each interacting with two charge-balancing framework Al sites in ZSM5.[18,20] Cu^+ ions are not likely to be stable in the Cu acetate solutions used for exchange, so exchanged Cu^+ species and Cu_2O crystallites are not likely to form during synthesis or during subsequent treatment in oxidizing environments (except as a result of autoreduction at very high temperatures). $\{Cu^{2+}–(OH)^-\}^+$ ions can also precipitate as $Cu(OH)_2$ crystallites but only at pH levels higher than those prevalent during ion exchange (above pH 6)[31] or they can crystallize from solution during drying; neither of these possibilities is likely because of the slightly acidic pH of the acetate solutions and because any residual Cu^{2+} ions within the catalyst agglomerates are removed during the multiple rinsing cycles. Thus, the formation of CuO and $Cu(OH)_2$ after exchange and thermal treatment is unlikely with our synthesis procedures. Indeed, three consecutive ion exchanges led to only a slight increase in Cu/Al ratios from 0.57 to 0.60 and finally to 0.61. This shows that the incorporation of Cu ions into the ZSM5 structure is limited by the number of exchange sites with sufficiently proximate Al framework cations that allow them to interact with one or two Cu^{2+} cations. If Cu species formed without association with zeolite (*e.g.*, as CuO or $Cu(OH)_2$), they would continue to form during sequential exchange cycles.

Monomeric Cu^{2+} species can exist as $\{Cu^{2+}–(OH)^-\}^+$ (I) or as Cu^{2+} monomers (II) (Fig. 1). Species (I) has been detected only after low-temperature thermal treatments of exchanged samples,[30,32,33] even though statistical isolation of some $\{Cu^{2+}–(OH)^-\}^+$ from other such species or from acidic OH would prevent their dehydration to form $\{Cu^{2+}–O^{2-}–Cu^{2+}\}^{2+}$ or Cu^{2+} species, unless $\{Cu^{2+}–(OH)^-\}^+$ species and associated framework Al sites become mobile during thermal treatment. The probability of dimer formation increases with increasing Cu/Al ratio; the presence of these dimers has been inferred from the removal of oxygen atoms from exchanged samples *via* autoreduction in He and *via* formation of H_2O and CO_2 during reduction with H_2 and CO respectively.[18,20] In the next section, we examine the reaction of Cu-ZSM5 with H_2 and the kinetics and stoichiometry of Cu^{2+} reduction and of H_2O formation with increasing temperature.

Reduction of Cu^{2+} species in Cu-ZSM5 using H_2

H_2 consumption and H_2O formation rates on Cu(0.12), Cu(0.36), Cu(0.58), and Cu(0.60) samples are shown as a function of temperature in Fig. 2. Two H_2 consumption peaks centered at ~450 K and ~650 K were detected in all samples. These data differ from some previously reported results, in which three distinct peaks were reported for Cu-ZSM5 samples with Cu/Al ratios (0.75) similar to some of the samples in Fig. 2.[18] The third peak in these samples appeared near ambient temperatures and it was assigned to the reduction of Cu^{2+} dimers (Species III).[18] In our experiments, the temperature ramp started at ~220 K in order to ensure rigorous detection of any reduction processes occurring near ambient temperatures. In contrast with previous studies, we failed to detect

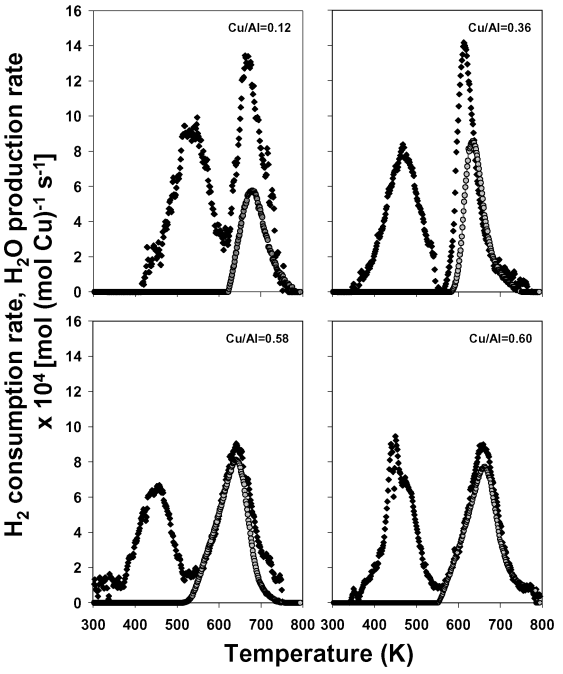

Fig. 2 Temperature programmed reduction in 5% H_2/Ar (0.417 cm^3 s^{-1}) at 0.167 K s^{-1}, for different Cu/Al ratios (0.2 g), (◆) hydrogen consumption rate, and (●) H_2O production rate.

any H_2 consumption or any H_2O formation below 400 K. We did detect an initial decrease in the H_2 gas phase concentration upon switching from He to the H_2 mixture, irrespective of the temperature at which the switch occurs; this peak was observed even on Na-ZSM5 and H-ZSM5. It arises from the replacement of He held within zeolite channels with the H_2-containing mixture, which leads to the net removal of some H_2 from the reactant gas stream. The evolution of H_2O coincided with the H_2 consumption peak at ~650 K (Fig. 2).

Before proceeding with the assignment of these two peaks to specific reduction processes and Cu^{2+} species, we consider first the amount of H_2 consumed (H_2/Cu) and the amount of H_2O formed (H_2O/Cu) indicated by the data in Fig. 2 and shown in Table 2. At all Cu/Al ratios (in the 0.12–0.60 range), the total H_2/Cu ratio was 0.97–1.01, indicating that all the Cu^{2+} ions have undergone a two-electron reduction to Cu^0 by the final treatment temperature (773 K). The total amount of H_2 consumed is equally distributed between the two reduction peaks, each one of which corresponds to ~0.5 H_2/Cu (Fig. 2). This suggests that all Cu starts in oxidation state 2+, reduces fully to Cu^+ during the first reduction peak and to Cu^0 during the second reduction peak. This result also confirms that the O_2 treatment used for all samples before reduction leads to the stoichiometric formation of Cu^{2+} without any detectable autoreduction. The amount of H_2O evolved ranges from 0.26 to 0.46 H_2O/Cu for the various samples and it increases with increasing Cu/Al ratio (Table 2). H_2O can form *via* removal of oxygen atoms from oxygen-containing Cu species, but also *via* recombination of zeolitic OH groups during incipient dealumination of the zeolite. Before reduction of Cu^+ species, negligible amounts of OH groups exist at exchange sites, but vicinal OH groups form *via* subsequent reduction of Cu^+ species, which were in turn formed *via* reduction of oxygen-bridged Cu^{2+} dimers and isolated Cu^{2+}. The measured H_2O amounts contain H_2O formed both from reduction of Cu dimers and from dealumination of the zeolite; therefore, these measurements overestimate slightly the number of removable oxygen atoms from Cu species.

Table 2 H_2 consumption and H_2O production stoichiometry from H_2 TPR

Catalyst	Cu(0.12)[a]	Cu(0.36)	Cu(0.38)	Cu(0.58)	Cu(0.60)
H_2/Cu					
Peak 1	0.51	0.48	0.44	0.45	0.48
Peak 2	0.53	0.50	0.53	0.52	0.53
Total	1.04	0.98	0.97	0.97	1.01
H_2O/Cu	0.26	0.30	0.31	0.45	0.46
H_2O/H_2 (2nd peak)	0.49	0.60	0.58	0.86	0.88

[a] Molar ratio of Cu to total Al.

Next, we consider the stoichiometry for the complete reduction of each of the four species shown in Fig. 1 in order to probe their potential respective contributions to the two reduction peaks shown in Fig. 2. The stoichiometries expected for the various Cu species in Fig. 1 are shown in eqns. (1)–(4) (in Table 3). All four species start as Cu^{2+} species and reduce to Cu^0 with equal amounts of hydrogen consumption (H_2/Cu = 1). Thus, these four species differ only in their relative rates of H_2O formation and in their oxygen content.

The area under the high-temperature H_2 consumption is similar in all samples (H_2/Cu = 0.50–0.53), but that of the coincident H_2O evolution peak differs among samples with different Cu/Al ratios (Table 2). This indicates that only some of the H_2 consumed in this peak leads to the H_2O formed, and that H_2 is used to reduce more than one type of Cu species, albeit with similar reduction kinetics. The H_2O/Cu ratio is less than 0.5 for all samples, which precludes the exclusive presence of dimers and CuO, which would lead to H_2O/Cu ratios of 0.5 and 1 (eqns. (1)–(4) in Table 3), respectively. Thus, Cu^{2+} monomers at exchange sites, which would reduce to Cu^0 with the concurrent formation of protons (but not H_2O), must be present in all Cu-ZSM5 samples. If crystalline CuO were present, its reduction would occur at relatively low temperatures (~500 K),[20] and its coincidence with the H_2O evolution peak from dimers would be unlikely. The H_2O/Cu ratio increases with increasing Cu/Al ratio (Table 2), suggesting that the oxygen removed as H_2O arises from Cu species that become more abundant as the distance among Cu cations decreases. This is consistent with the expected prevalence of Cu dimers as Cu/Al ratios increase. The only other species with extraframework oxygen atoms is $\{Cu^{2+}(OH)^-\}^+$, but its relative abundance should decrease as the probability of finding isolated Cu species decreases with increasing Cu/Al ratio; moreover, the reduction of $\{Cu^{2+}(OH)^-\}^+$ would lead to H_2O/H_2 ratios of 1. The relative abundance of $\{Cu^{2+}–O^{2-}–Cu^{2+}\}^{2+}$ dimers should increase with increasing density of $\{Cu^{2+}(OH)^-\}^+$ species initially formed during ion exchange in slightly acidic media, because such species are more likely to condense with similar species and less likely to react with a decreasing number of remaining OH groups to form instead Cu^{2+} cations bridging two exchange sites. The prevalence of dimers at higher Cu/Al contents is consistent with the higher H_2O/Cu values measured at higher Cu/Al ratios, which reflect a larger contribution from reduction events occurring that remove oxygen atoms instead of forming protons.

In view of these results, we attempt to describe H_2 reduction processes (Fig. 2) using only exchanged Cu^{2+} and $\{Cu^{2+}–O^{2-}–Cu^{2+}\}^{2+}$ species (Fig. 3). The H_2/Cu ratios (0.50–0.53 for all samples) from the second reduction peak indicates that this step reduces every Cu atom in the sample from Cu^+ to Cu^0; in turn, this suggests the complete reduction of Cu^{2+} to Cu^+ within the first H_2 consumption peak for both Cu^{2+} monomers and $\{Cu^{2+}–O^{2-}–Cu^{2+}\}^{2+}$ dimers. The incipient reduction of cations in metal oxides is often limited by the rate of initial H_2 dissociation; therefore, the observed coincident reduction of two structurally distinct species within this first peak may only reflect the temperature required for the incipient

Table 3 Stoichiometry for H_2 reduction, for different copper species

Copper species	Reaction	H_2O/Cu
$\{Cu^{2+}–(OH)^-\}^+$	$\{Cu^{2+}–(OH)^-\}^+ + H_2 \rightarrow Cu^0 + H^+ + H_2O$ (1)	1
Cu^{2+}	$Cu^{2+} + H_2 \rightarrow Cu^0 + 2H^+$ (2)	0
Copper dimers $\{Cu^{2+}–O^{2-}–Cu^{2+}\}^{2+}$	$\{Cu^{2+}–O^{2-}–Cu^{2+}\}^{2+} + 2H_2 \rightarrow 2Cu^0 + 2H^+ + H_2O$ (3)	0.5
Bulk copper oxide[18,20]	$CuO + H_2 \rightarrow Cu^0 + H_2O$ (4)	1

formation of H-atoms required for the reduction of both types of Cu species.

H_2O desorbs only at higher temperatures, in a peak coincident with the second H_2 reduction peak. This water is not just adsorbed on ZSM5, because during initial pretreatments in oxygen or He, H_2O evolves at much lower temperatures (350–400 K). Yet, during H_2-TPR, water does not desorb after Cu^{2+} is reduced to Cu^+, apparently because of the presence of a H_2O binding site on the Cu^+ species formed. As Cu^+ is subsequently reduced to Cu^0, this binding site is destroyed and all of the water formed during reduction desorbs at the same temperature (and apparently *via* the same kinetic process) as the second H_2 consumption peak.

X-Ray absorption spectroscopy during reduction of Cu-ZSM5 in H_2

These conclusions were confirmed by X-ray absorption spectra measured during treatment in H_2. The near-edge spectral region is sensitive to the Cu oxidation state.[9–11,34–38] Fig. 4a and 4b shows near-edge spectra for Cu(0.38) during reduction in H_2 at increasing temperatures. Two spectral features (labeled (I) and (II); Fig. 4a and 4b) changed during H_2 treatment. The intensity of (I) increased with temperature up to 523 K, as (II) became weaker (Fig. 4a). Between 523 K and 800 K, (I) became less intense and ultimately disappeared (Fig. 4b), suggesting a change in the oxidation state of Cu atoms. These changes in the near-edge spectra may reflect the reduction of Cu^{2+} to Cu^+ and then to Cu^0. In fact, the feature at 8983–8984 eV for species (I) has been assigned to dipole-allowed $1s \rightarrow 4p$ electronic transitions in Cu^+.[9,34–39] In contrast, Cu^{2+} species show three features in the near-edge region: a weak absorption at about 8978 eV, attributed to dipole-forbidden $1s \rightarrow 3d$ transitions and a shoulder at 8988 eV and an intense peak at 8998 eV, both arising from $1s \rightarrow 4p$ transitions.[9,34–39] During reduction, additional electrons are placed onto unoccupied Cu atomic orbitals, leading to changes in the probability of core s-electron transitions into these valence bound states.[35]

Near-edge X-ray absorption spectra for Cu(0.38) (Spectra A–C) and for a Cu foil (Spectrum D) are shown in Fig. 5. No significant features were detected in the Cu(0.38) sample exposed to ambient air (Spectrum A), apparently as a result of significant structural distortion by coordinated water, which provides confirming evidence for the dispersed nature of Cu^{2+} species in fresh samples. In contrast, the spectra during treatment in O_2 showed features corresponding to Cu^{2+} (Spectrum B). Spectrum C corresponds to the sample (Cu(0.38)) after reduction in H_2 at 523 K, a temperature that lies between the two H_2 consumption peaks (Fig. 2). Spectrum C has a distinct feature that is absent in Spectra B and D and which has been attributed to Cu^+ species.[10,34]

The two well-defined and equimolar H_2 consumption peaks during H_2 reduction (Fig. 2) suggest that reduction occurs in two sequential and well-defined one-electron reduction steps leading to Cu^0 at the end of the process. This sequential $Cu^{2+} \rightarrow Cu^+ \rightarrow Cu^0$ process is consistent with the near-edge spectra in Fig. 5 and with the transient evolution of the near-edge spectra (Figs. 4a and 4b). Feature (I) at ~8983 eV, attributed to Cu^+, first increased and then decreased with increasing temperature. The magnitude of these changes was estimated by linear combination methods using the starting spectrum, the intermediate spectrum between the two reduction peaks, and Cu foil as standards for Cu^{2+}, Cu^+, and Cu^0 species, respectively. The corresponding fitted spectra for two samples are shown in Fig. 6, along with the experimental

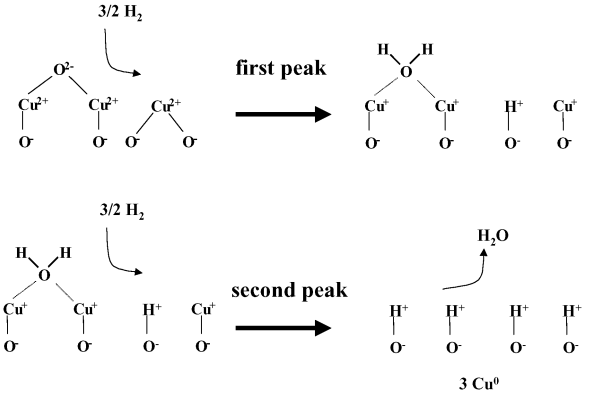

Fig. 3 Stoichiometry and pathways for reduction of Cu^{2+} and $\{Cu^{2+}–O^{2-}–Cu^{2+}\}^{2+}$ in Cu–ZSM–5 using H_2 as the reductant.

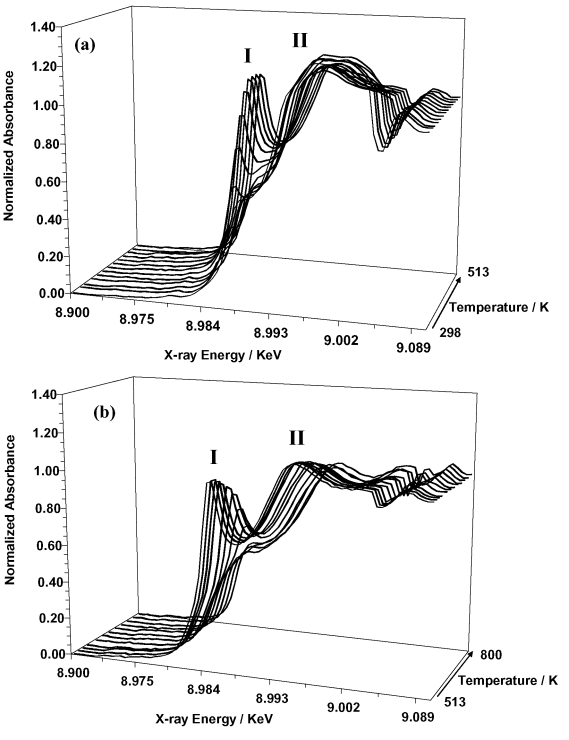

Fig. 4 X-ray absorption near-edge spectra after *in situ* temperature programmed reduction of Cu(0.38) in 5% H_2/Ar (a) from room temperature to 523 K and (b) from 523 K to 823 K at 0.067 K s^{-1}. The energy-scale is expanded between 8.975 and 9.002 keV in order to show the edge region in greater detail.

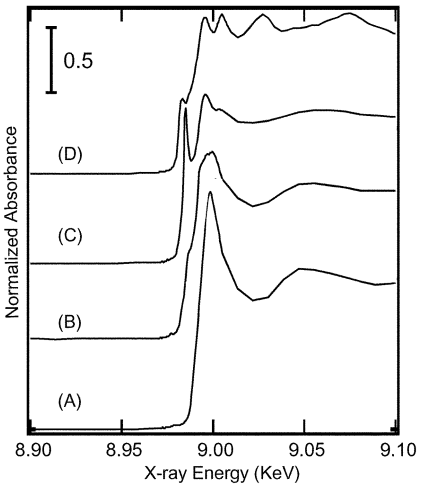

Fig. 5 X-ray absorption near-edge spectra, (A) Cu(0.38) fresh exposed to ambient air, (B) Cu(0.38) in 50% O_2/He at 773 K, (C) Cu(0.38) in 5% H_2/Ar at 523 K, (D) reference Cu foil at 298 K.

spectra. During H_2 treatment at 475 K (Fig. 6a), the sample consists of nearly equimolar amounts of Cu^{2+} and Cu^+, while at 648 K (Fig. 6b), the Cu^+ fraction is ~0.75. From the good agreement between the experimental and fitted spectra, it is clear that the intermediate spectra can be represented accurately by linear combinations of the standard spectra.

The evolution of the various Cu species estimated from these linear combination analysis methods can be compared with the rates of H_2 consumption and H_2O evolution measured from mass spectrometric analysis of the effluent during reduction in H_2 (Fig. 7). Fig. 7a and 7c show the H_2-TPR profiles and the relative amounts of each Cu species obtained from the X-ray absorption spectra for Cu(0.38); Fig. 7b and 7d show the corresponding data for Cu(0.12). Principal component

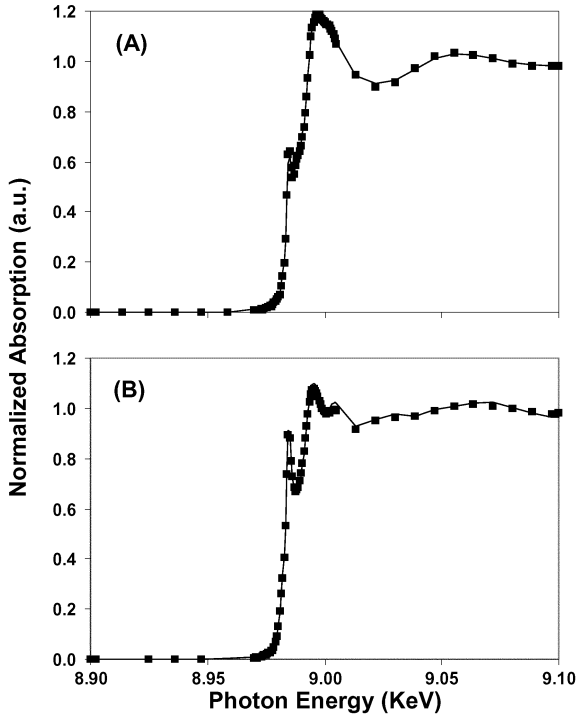

Fig. 6 Linear combination fit of X-ray absorption near-edge spectra during *in-situ* temperature programmed reduction in 5% H_2/Ar of Cu(0.38) at (A) 475 K and (B) 648 K. Lines represent the fitted spectra and ■ represent experimental spectra.

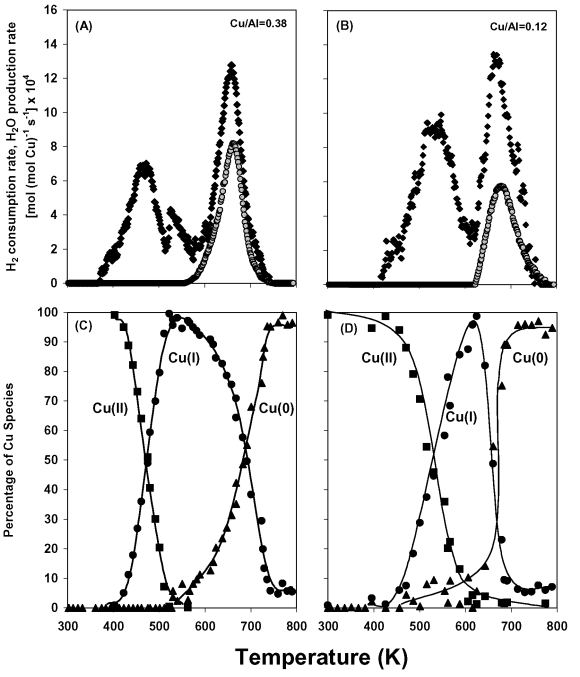

Fig. 7 Comparison between H_2 consumption rates and principal component analysis deconvolution of X-ray absorption near-edge spectra during *in situ* temperature programmed reduction of Cu(0.38) (A) and (C) and Cu(0.12) (B) and (D). For (A) and (B), ◆ represents the hydrogen consumption rate, and ● represents the H_2O production rate. For (C) and (D), ■ represents Cu(II), ● represents Cu(I), ▲ represents Cu(0).

analysis showed that these are complete fits for Cu(0.38), without any omitted structures and with all the Cu^{2+} species initially present converted fully to Cu^0 by the final temperature.

The structural description of Cu(0.12) is less straightforward than for Cu(0.38). Principal component analysis suggests that the Cu(0.12) starting material contains more structural features than Cu(0.38) or that the structures of these Cu^{2+} species change with temperature. The Cu^+ intermediate formed at ~620 K in Cu(0.12) is identical in structure to that formed in Cu(0.38) at the same temperature and it accounts for all of the initial Cu^{2+} in the starting material. As also suggested by Fig. 4, Cu^+ reaches a maximum concentration near the end of the low-temperature H_2 consumption peak. After the high temperature reduction peak (at ~800 K), the sample is more than 95% Cu^0. This apparent incomplete conversion reflects differences in the near-edge spectrum between the Cu foil standard and the small Cu^0 clusters likely to form after reduction of exchanged Cu cations, and not the incomplete reduction of these Cu species. This was confirmed by extended X-ray absorption fine-structure (EXAFS) analysis. Cu atoms in metal clusters formed during reduction at ~550–750 K showed a Cu–Cu first-shell coordination number of 6–7. Cu atoms in a 7.6 Å cluster with one core Cu atom and a complete shell of 12 neighbors would have an average Cu–Cu coordination number of 5.5. This suggests that the Cu metal clusters are small (~10 Å) and completely reduced after treatment in H_2 at ~800 K.

Reduction of Cu^{2+} species in Cu-ZSM5 using CO and further reduction in H_2 after CO treatment

The number of Cu species with removable oxygens (*e.g.*, CuO and Cu dimers) were also measured from the evolution of CO_2 during reduction of Cu-ZSM5 in CO, as also reported previously.[20] The H_2-TPR data showed that CuO clusters were not present and that removable oxygen atoms were exclusively

associated with $\{Cu^{2+}–O^{2-}–Cu^{2+}\}^{2+}$ dimers. Cu^{2+} monomers cannot reduce with CO, because protons are unavailable for the required charge balance. Thus, CO_2 forms only from oxygen atoms in $\{Cu^{2+}–O^{2-}–Cu^{2+}\}^{2+}$ species *via* the reaction:

$$\{Cu^{2+}–O^{2-}–Cu^{2+}\}^{2+} + CO \rightarrow 2Cu^{+} + CO_2 \qquad (5)$$

The amount of CO_2 formed reflects the number of Cu dimers in each sample.

CO_2 formation rates on Cu(0.38), Cu(0.58), Cu(0.12), Cu(0.36), and Cu(0.60) are shown in Fig. 8 as a function of temperature. The onset of reduction is ~320 K for all of the catalysts except in Cu(0.12), for which the reduction begins at ~380 K. Poorly resolved features were detected between 350 K and 650 K in all samples; they appear to include two or three unresolved peaks, in contrast with the two distinct peaks previously reported at ~400 K and ~550 K for Cu/Al ratios similar to those in the present study.[18,20] These two peaks were assigned to $\{Cu^{2+}–O^{2-}–Cu^{2+}\}^{2+}$ and CuO, respectively, but our data are not consistent with these conclusions, because our samples lack CuO clusters, but yet exhibit similarly complex reduction behavior. The broad maximum in these features shifts from ~450 K for Cu(0.38) and Cu(0.58) to ~550K on Cu(0.60).

The formation of CO_2 requires CO adsorption and reaction with oxygen atoms in $\{Cu^{2+}–O^{2-}–Cu^{2+}\}^{2+}$. The broad CO_2 evolution profile may reflect the presence of $\{Cu^{2+}–O^{2-}–Cu^{2+}\}^{2+}$ dimers with different reactivity towards CO, either because of their local coordination to two exchange sites of varying structure or because of their non-uniform distances from CO adsorption sites. In contrast, all dimers, and even the Cu^{2+} monomers, reduced to Cu^{+} in a single narrow peak when H_2 was used as a reductant, apparently because reduction with H_2 is controlled by the kinetics of H_2 dissociation, and not by the non-uniform reactivity of Cu cations with the spilled-over hydrogen atoms. The non-uniform reactivity of $\{Cu^{2+}–O^{2-}–Cu^{2+}\}^{2+}$ structures inferred from the broad CO reduction profiles is confirmed below from the non-reactive desorption of O_2 from such structures.

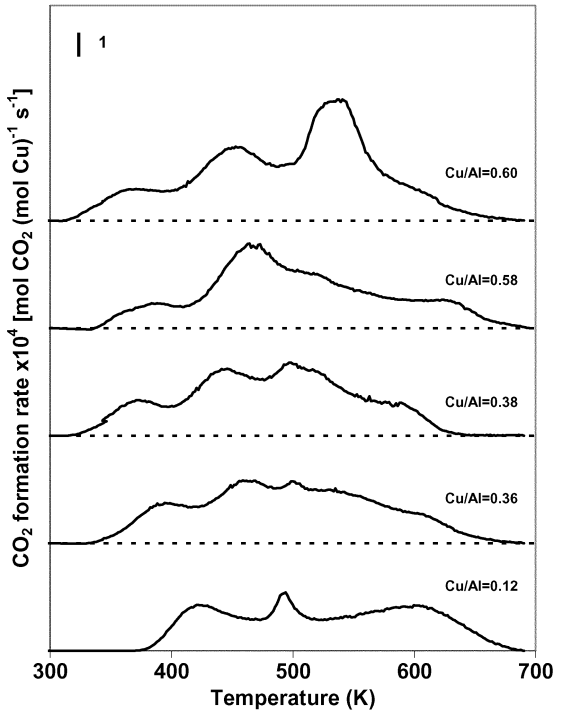

Fig. 8 CO_2 formation rates during temperature programmed reduction in 1% CO/He (0.5 cm^3 s^{-1}) as a function of temperature (0.167 K s^{-1}) for all Cu/Al ratios (0.2 g).

Table 4 Oxygen removal calculation from CO-TPR and comparison with the H_2-TPR on oxygen treated samples

Catalyst	Cu(0.12)	Cu(0.36)	Cu(0.38)	Cu(0.58)	Cu(0.60)
CO_2/Cu from CO-TPR	0.23	0.28	0.30	0.35	0.39
O/Cu from CO-TPR[a]	0.23	0.28	0.30	0.35	0.39
Cu_{dimer}/Cu	0.46	0.56	0.60	0.70	0.78
Cu_{dimer}/Al	0.055	0.20	0.23	0.41	0.47
Cu^{2+}/Al	0.065	0.16	0.15	0.17	0.13
$(O/Cu)^a/(O/Cu)^{b\,c}$	0.88	0.93	0.97	0.78	0.85

[a] Oxygen per total copper measured from the CO-TPR (final temperature 700 K). [b] Oxygen per total copper measured from the H_2-TPR (final temperature 800 K). [c] Ratio of the oxygen removal during the CO-TPR and the H_2-TPR.

The CO_2/Cu ratios during reduction of Cu-ZSM5 by CO range from 0.23 for the low Cu/Al ratio sample to 0.39 for the sample with highest Cu/Al ratio (Table 4). The number of O-atoms removed as CO_2 is slightly smaller than the number removed as H_2O during reduction in H_2, because small amounts of H_2O can also be formed *via* condensation of zeolite OH groups, as vicinal OH groups form during reduction of $\{Cu^{2+}–O^{2-}–Cu^{2+}\}^{2+}$. As a result, CO_2/Cu ratios provide a more direct measurement of the number of Cu dimers than H_2O/Cu ratios. The Cu_{dimer}/Cu fraction is twice the value of this CO_2/Cu ratio because each O-atom is associated with 2 Cu atoms. We conclude that between 46% and 78% of the Cu atoms are present as Cu dimers in our samples (Table 4); this percentage increases with increasing Cu/Al ratio, as expected from the shorter average distance among Cu atoms at higher Cu/Al ratios.

These conclusions about Cu speciation were confirmed by reducing samples in H_2 after CO-TPR (and cooling in CO to ambient temperature). The H_2 consumption, H_2O formation, and CO desorption rates are shown in Fig. 9 for Cu(0.36). Two H_2 consumption peaks were observed (at ~600 K and ~750 K), while H_2-TPR studies after CO-TPR previously reported a single reduction peak at 800 K,.[18,20] This peak was attributed to reduction of Cu^{+} species formed *via* reactions of Cu^{2+} monomers with Cu metal species, which had been formed by reduction of CuO to Cu using CO.[20] These complex pathways would require the migration of Cu metal at relatively low temperatures and would not occur when CuO clusters are not present. The two H_2 consumption peaks appear at slightly higher temperatures (Fig. 9) than during reduction of fresh samples in H_2 (Fig. 2). This reflects the adsorption of CO on Cu^{+}, as previously detected by infrared spectroscopy.[18,40] During H_2-TPR, CO desorbs at ~700 K (see insert in Fig. 9), immediately before the second H_2 consumption peak. Thus, the stability of Cu^{+}(CO) appears to delay the onset of reduction compared to free Cu^{+} cations. Below, we show that the amounts of H_2 consumed, of H_2O formed, and of CO desorbed during H_2-TPR are consistent with the Cu distribution measured from CO reduction.

The first H_2 consumption peak during reduction of air-treated samples in H_2 (Fig. 2) corresponds to the reduction of both $\{Cu^{2+}–O^{2-}–Cu^{2+}\}^{2+}$ and Cu^{2+} monomers to Cu^{+}. During reduction in CO, all $\{Cu^{2+}–O^{2-}–Cu^{2+}\}^{2+}$ species can reduce to Cu^{+}, but Cu^{2+} monomers remain as divalent cations. Thus, the first H_2 consumption peak in samples pre-treated in CO (Fig. 9) must reflect the reduction of Cu^{2+} monomers. The area under this peak provides an independent estimate of the fraction of Cu^{2+} initially present as monomers. These monomer Cu^{2+}/Cu_{total} estimates are 0.38 for Cu(0.36), in relatively good agreement with the value of 0.44 measured from CO

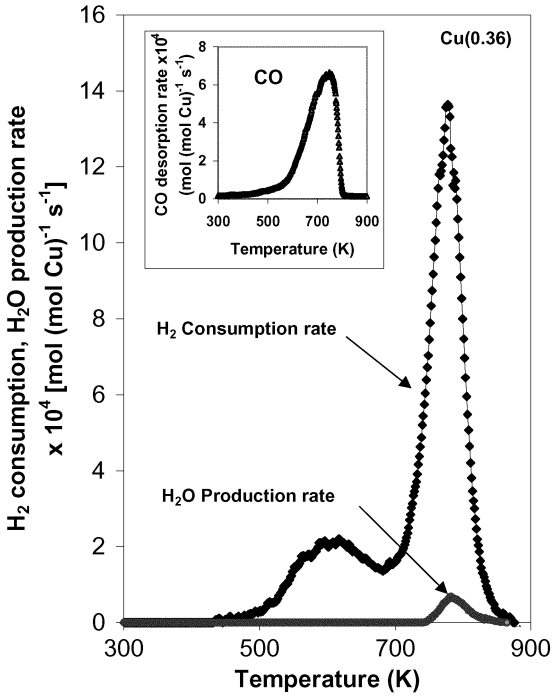

Fig. 9 Temperature programmed reduction in 5% H_2/Ar (0.417 cm^3 s^{-1}) at 0.167 K s^1, after CO TPR experiments in Fig. 10 for Cu(0.36) sample (0.2 g), (◆) hydrogen consumption rate, and (●) H_2O production rate.

reduction data (Table 5). The second reduction peak in Fig. 9 gives a H_2/Cu of 0.50 for Cu(0.36) (Table 5), as also obtained from the second H_2 reduction peak in O_2-treated samples. This confirms that the second peak in both cases (initial H_2 reduction and H_2 reduction after CO treatments) corresponds to the stoichiometric reduction of every Cu atom from Cu^+ to Cu^0. Finally, the amount of CO desorbed during reduction in H_2 of CO-treated samples (0.57 CO/Cu; Fig. 9) is almost identical to the number of Cu atoms in dimers estimated from CO reduction of this sample after air treatment (0.56 Cu_{dimer}/Cu) (Table 5). This confirms that all Cu-dimers are reduced to vicinal Cu^+ species during CO-TPR at 700 K, and that each of these Cu^+ adsorbs one CO during cooling to ambient temperature in CO.

A small amount of H_2O desorbs concurrently with the second H_2 consumption peak (Fig. 9). This appears at first glance to contradict the conclusion that all O atoms in $\{Cu^{2+}$–O^{2-}–$Cu^{2+}\}^{2+}$ were removed during the preceding treatment in CO. The reduction of Cu^+ (ex-dimers) to Cu^0 and also of isolated Cu^{2+} to Cu^0 with H_2 leads to the formation of OH groups as vicinal pairs; these vicinal OH groups can readily react to form H_2O in condensation reactions that remove framework oxygens and lead to incipient zeolite dealumination. This process also occurs during reduction of fresh samples in H_2 and it is responsible for the slightly larger amounts of oxygen removed during reduction in H_2 compared with the amounts of oxygen removed by reduction in CO. We can bring the results of H_2 and CO reduction measurements into excellent agreement by subtracting the amount of H_2O formed *via* dehydroxylation from the corresponding amounts formed during reduction in H_2. After this correction, the amount of oxygen removed as water from dimers using H_2 is 0.275 H_2O/Cu, while that removed by CO as CO_2 is 0.280 CO_2/Cu.

The results of these three types of experiments (H_2-TPR, CO-TPR, and H_2-TPR after CO-TPR) and the amounts of CO adsorbed on CO-treated samples provide a remarkably consistent picture of the Cu speciation in these samples. The distribution of Cu species is also consistent with the expected distribution of Al–Al next nearest neighbors in these ZSM5 samples, as discussed below.

Distributions of Al–Al pairs

The highest Cu_{dimer}/Al ratio determined from CO-TPR measurements was 0.47 (for Cu(0.60)), while the highest $Cu_{monomer}$/Al ratio was 0.17 (for Cu(0.58)) (Table 4). Both dimers and monomers must interact with two Al sites in ZSM5. Here, we examine whether the proposed Cu speciation is consistent with the expected distribution of Al–Al pairs in ZSM5 samples with the Si/Al ratios in our sample.[41–43]

The maximum Al–Al distances that Cu monomers and Cu dimers can span are not directly available, so we must estimate them from Cu–Al and Cu–Cu distances in known Cu compounds. Cu–Al distances in isolated $Cu^{2+}(OH)^-$ have been calculated to be 2.72 Å[43] using density functional theory methods. Cu–Cu distances of 2.95 Å have been reported in CuO from X-ray absorption data.[9] For Cu dimers, estimates of Al–Al distances through the Al–O–Cu–O–Cu–O–Al bonds depend on bond angles. Using Al–Cu and Cu–Cu distances cited above, the maximum Al–Al distance for Cu dimers would be ~8.4 Å (the sum of 2.72 Å, 2.95 Å, and 2.72 Å). From Al–Al statistics[42] and the Si/Al ratio of ~14 in our samples, we conclude that 0.47 Cu_{dimer}/Al (the maximum experimental value) can be located using Al–Al distances between 5.5 and 6 Å (Fig. 4 in ref. 42). Since these Cu dimers can use even more distant Al–Al pairs (up to ~8.4 Å), the observed number of dimers can be easily accommodated within the Al–Al pairs available in the ZSM5 samples used here.

Most Cu^{2+} monomers appear to prefer locations within flat 5-membered rings in ZSM5 (~75% of the Cu^{2+} for random Al placement, and ~60% for equilibrium Al placement).[42] For a Si/Al ratio of 14, these flat 5-membered T-site rings have a maximum M^{2+}/Al of 0.14 when Al sites are placed randomly in the ZSM5 structure and 0.09 when Al atoms are distributed according to their energies at various T-sites. Our monomer Cu^{2+}/Al ratios for the samples with the highest Cu contents are between 0.13 and 0.17, in agreement with the predictions for random Al placement. Other types of rings can also stabilize Cu^{2+} cations, leading to slightly higher monomer Cu/Al ratios.

Table 5 Cu species calculated from H_2 TPR after O_2 (50% O_2/He) or CO (1% CO/He) treatment for the catalyst Cu(0.36)

	O_2 pretreatment	CO TPR	Difference	Cu-dimer fraction
CO_2/Cu formed during CO TPR	0.00	0.28	0.28	0.56
H_2/Cu consumed				
Peak 1	0.48	0.19	0.29	0.58
Peak 2	0.50	0.50	0	
Total	0.98	0.69	0.29	0.58
H_2O/Cu formed	0.30	0.025	0.275	0.55
CO/Cu desorbed during H_2-TPR	0.00	0.57	0.57	0.57

The measured monomer Cu^{2+}/Al ratios (from CO reduction) are relatively constant for all samples (0.13–0.17), except at the lowest Cu/Al ratio. It appears that sites capable of stabilizing a Cu^{2+} saturate first during ion exchange and that further exchange titrates remaining sites too distant for monomer stabilization, but able to interact with the more distant Cu ions in an oxygen-bridged dimer. As the Cu content increases, sites capable of stabilizing these dimers are also depleted, as evidenced by asymptotic ratios of ~0.60 Cu/Al obtained after multiple sequential exchanges.

The speciation of Cu inferred from these various methods for oxygen-treated and reduced samples lead to a relatively simple picture. Dispersed Cu^{2+} and $\{Cu^{2+}–O^{2-}–Cu^{2+}\}^{2+}$ account for all Cu species in the samples and their relative concentrations are consistent with the expected Al–Al radial distributions in these ZSM5 samples. In the next section, we explore the autoreduction of $\{Cu^{2+}–O^{2-}–Cu^{2+}\}^{2+}$ and the possible existence of dimers with varying structure and reactivity.

O_2 Evolution and autoreduction of $\{Cu^{2+}–O^{2-}–Cu^{2+}\}^{2+}$ in He

O_2 evolution profiles are shown in Fig. 10 as a function of temperature for Cu–ZSM5 samples with varying Cu/Al ratios. For Cu/Al ratios greater than 0.12, O_2 desorbs in a narrow peak at ~673 K, followed by a broader desorption feature at higher temperatures. The first peak shifts slightly to higher temperatures for Cu(0.12) (~735 K). The O_2-TPD profiles for samples with Cu/Al ratios greater than 0.12 are consistent with previous studies.[17,44,45] Small O_2 desorption peaks have been reported at low temperatures and may reflect low coverages of molecularly adsorbed oxygen or even the diffusion of O_2 molecules within zeolite channels.[17,44–46] The number of oxygen atoms removed should correspond to the number of $\{Cu^{2+}–O^{2-}–Cu^{2+}\}^{2+}$ dimers able to recombine oxygen atoms at each temperature. The amounts of oxygen removed (O/Cu) during desorption in He are shown in Table 6 for all samples. For Cu(0.58), the O/Cu ratio is 0.20, in agreement with previous reports[17] for Cu–ZSM5 with similar Cu/Al ratios (0.57). The O/Cu ratios obtained from these desorption data, however, are much smaller than those obtained from the CO_2 formed during reduction in CO (0.35 O/Cu); thus, not all $\{Cu^{2+}–O^{2-}–Cu^{2+}\}^{2+}$ dimers autoreduce, even at ~1100 K. The fraction of the Cu-dimers that desorbs O-atoms as O_2 increased with increasing Cu/Al ratio (from 35% in Cu(0.12) to 57% in Cu(0.58); Table 6). As Cu dimers become more distant with decreasing Cu/Al ratio, the probability of recombination decreases. Isolated Cu dimers do not appear to be able to reduce at all without a reductant capable of removing oxygen as H_2O or CO_2 (or as NO_2 during catalytic NO decomposition).

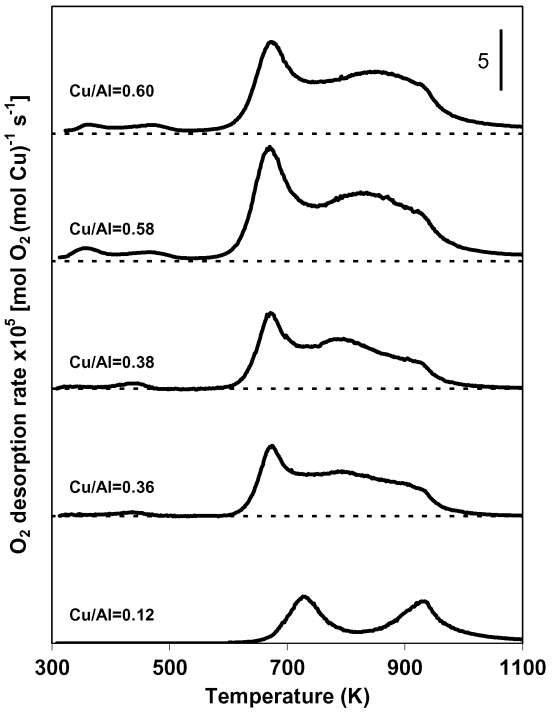

Fig. 10 Oxygen desorption rate in He (0.5 cm^3 s^{-1}) as function of temperature (0.167 K s^{-1}) for all the Cu/Al catalysts (0.2 g), after treatment in oxygen at 773 K.

Table 6 Oxygen removal calculation from O_2-TPD, and comparison with CO-TPR

Catalyst	Cu(0.12)	Cu(0.36)	Cu(0.38)	Cu(0.58)	Cu(0.60)
O/Cu from O_2-TPD[a]	0.08	0.13	0.14	0.20	0.20
O/Cu from CO-TPR[b]	0.23	0.28	0.30	0.35	0.39
$(O/Cu)^a/(O/Cu)^{b\,c}$	0.35	0.46	0.47	0.57	0.51

[a] Oxygen per total copper measured from the O_2-TPD (final temperature 1100 K). [b] Oxygen per total copper measured from the CO-TPR (final temperature 700 K). [c] Ratio of the oxygen removal during the O_2-TPD and the CO-TPR.

Two O_2 desorption peaks are clearly visible on Cu(0.12), suggesting that two autoreduction mechanisms or two types of Cu dimers are responsible for the evolution of O_2 . At higher Cu/Al ratios, two peaks also seem to account for all O_2 evolution features (Fig. 10). O_2 evolution requires kinetic paths involving either vicinal oxygen atoms or the migration of oxygen atoms located beyond atomic distances. Thus, it seems plausible that the evolution of O_2 at low temperatures arises from vicinal Cu dimers, which can form O–O bonds without requiring diffusion. At higher temperatures, more distant dimers can communicate *via* migration of Cu dimers and their bridging oxygen, or at high temperatures, even *via* the formation and diffusion of oxygen radicals. Some, but not all of the Cu dimers, are able to autoreduce *via* these latter pathways as part of the high-temperature reduction processes observed in all samples (Fig. 10).

In order to probe these desorption pathways and to detect the migration of any Cu dimers, which would place them in temporary proximity to each other and lead to O_2 formation, we conducted three consecutive O_2 desorption experiments on Cu(0.60) with intervening O_2 treatment at 773 K between them (Fig. 11). Only the high-temperature desorption peak shifted (to lower temperatures) after each desorption cycle (up to 1100 K), without any detectable change in the amount of oxygen desorbed (O_2/Cu = 0.10). Thus, it appears that some migration of the Cu dimers occurs irreversibly and that this migration tends to decrease the average distance among the Cu dimers responsible for the high temperature desorption peak. The Cu dimers appear to retain their newly acquired proximity and to require lower temperatures for oxygen recombination during subsequent desorption cycles. A large fraction of the Cu dimers, however, is unable to undergo autoreduction even at the highest temperatures of our experiments. Such sites would also be unable to participate in redox cycles requiring recombinative desorption steps. Our recent results[22,23] have shown, however, that oxygen removal steps involving NO_2 formation and decomposition of NO_2 and the use of NO as an oxygen carrier among distant redox sites allow all dimers to participate in NO decomposition redox cycles, irrespective of their relative proximity.

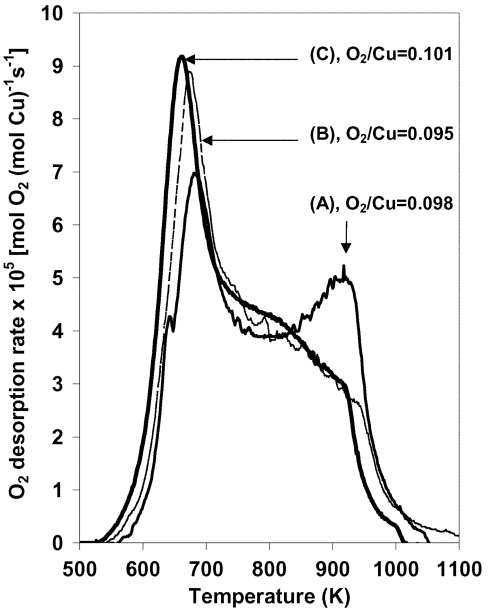

Fig. 11 Oxygen programmed desorption in He as a function of temperature for Cu(0.60), (A) first O_2-TPD after O_2 treatment at 773 K, (B) second O_2-TPD after the first one and a new O_2 treatment at 773 K, (C) third O_2-TPD after the second one and a new O_2 treatment at 773 K.

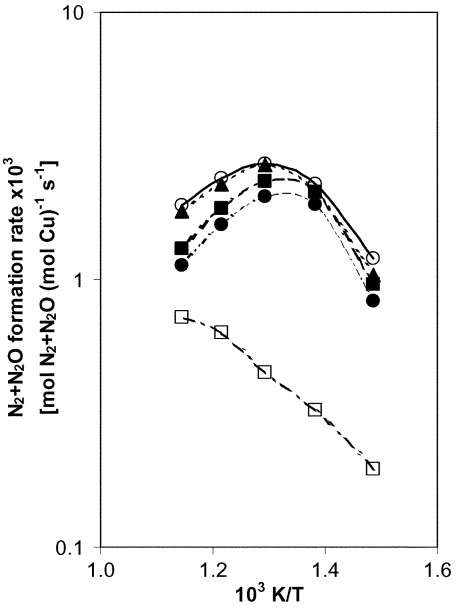

Fig. 12 Arrhenius plot of $N_2 + N_2O$ formation rates on samples with various Cu/Al ratios, (□ Cu(0.12), ■ Cu(0.38), ○ Cu(0.58) ● Cu(0.36), ▲ Cu(0.60)) during NO decomposition at 673–873 K and 1 kPa NO.

Dependence of catalytic NO decomposition rates on the number of Cu dimers and monomers

The mechanism of NO decomposition on Cu–ZSM5, which involves N_2O and NO_2 as intermediates for N_2 and O_2 formation, respectively, is discussed in detail elsewhere.[22,23] In this study, the NO decomposition rate data are correlated with the amounts of different Cu species in order to determine which Cu species are active for NO decomposition. Steady-state NO decomposition rates ($N_2 + N_2O$ formed per total Cu atom) are shown in Fig. 12 for all Cu-ZSM5 samples. Except on Cu(0.12), which gives lower rates and a monotonic increase in rate with increasing temperature, the temperature dependence of catalytic NO decomposition rates shows the usual patterns previously reported on Cu–ZSM5.[7,47] NO decomposition rates increase with temperature up to 773 K and then decrease at higher temperature. This behavior reflects a complex interplay between bimolecular surface decomposition steps with low activation energies and the unfavorable thermodynamics for NO adsorption on Cu^+ sites at high temperatures.[22] This rate decrease becomes detectable as Cu dimers become increasingly reduced at high temperatures.

In order to compare the rates for the various catalysts at the same gas phase composition, the rates were extrapolated to the inlet conditions (1 kPa NO, 0 kPa O_2) using the kinetic rate expression:

$$r = \frac{k_{app}[NO]^2}{1 + K_\alpha[O_2]^{1/2}} \quad (6)$$

and previously measured values of K_α.[22] K_α is the equilibrium constant for dissociative O_2 adsorption; it has a value of 3.2 $kPa^{-1/2}$ at 773 K on Cu(0.58).[22] Three other catalysts, Cu(0.36), Cu(0.38) and Cu(0.60), gave very similar rate expressions and temperature dependences as Cu(0.58) and we expect similar values of K_α. On Cu(0.12), however, the different temperature dependence (Fig. 12) indicates that K_α values are much higher than for the other samples, leading to the prevalence of oxidized Cu dimers even at temperatures above 800 K.

Catalytic NO decomposition rates per Cu atom increased with increasing Cu/Al ratio (Table 7), implicating Cu dimers, the fraction of which increases with increasing Cu/Al ratio, as the active species in NO decomposition turnovers. Turnover rates (per Cu^{2+} or Cu_{dimer}) calculated from the measured Cu speciation are also shown in Table 7. NO decomposition turnover rates based on the numbers of Cu dimers on Cu(0.58), Cu(0.60), Cu(0.38), and Cu(0.36) are very similar. In contrast, the apparent turnover rate based on Cu^{2+} monomers increases drastically with increasing Cu/Al ratio (Table 7), suggesting that such sites are not involved in NO decomposition turnovers.

The sample with the lowest Cu/Al ratio (Cu(0.12)), however, gives much lower turnover rates (per Cu dimer) than the other catalysts. This reflects the higher K_α value for this catalyst, which indicates that bridging oxygen atoms in the Cu dimers present on this catalyst are more stable and difficult to remove than in the other samples. As a result, redox cycles requiring the removal of these oxygen species are slower and the availability of reduced dimers for NO chemisorption much lower. It appears that the Cu dimers initially formed at low Cu contents prefer Al–Al pairs leading to very stable oxidized Cu dimers. This is consistent with the higher temperatures for the first O_2 desorption peak and first CO_2 formation peak on Cu(0.12) relative to the other samples. At higher Cu contents, dimers form less stable structures with weaker Cu–O bonds and lower enthalpies for oxygen adsorption, which lead to a higher steady-state density of reduced Cu species and to faster redox cycles. The difference in reducibility among Cu dimers of varying stability becomes less important at higher temperature, because reduced sites become the most-abundant surface species during reaction. At these higher temperatures, NO decomposition rates on Cu(0.12) approach those measured on the other samples (Fig. 12).

These data provide confirming evidence for the involvement of Cu dimers and of redox cycles in NO decomposition turnovers.[22,23] The removable oxygen atoms present in $\{Cu^{2+}$–O^{2-}–$Cu^{2+}\}^{2+}$, but not in isolated Cu^{2+}, are required for rapid redox cycles during NO decomposition. Some reactivity differences among prevalent dimers structures are clearly observed, indicating the presence of $\{Cu^{2+}$–O^{2-}–$Cu^{2+}\}^{2+}$ with a range of stability and oxygen binding energy.

Table 7 Correlation between the $N_2 + N_2O$ formation rates during the NO decomposition at 773 K (1 kPa NO) and the copper species on different Cu–ZSM5 catalysts

Catalyst	$N_2 + N_2O$ rate $\times 10^3$ per Cu (mol (mol Cu)$^{-1}$ s^{-1})	$N_2 + N_2O$ rate $\times 10^3$ per Cu_{dimer}(mol (mol Cu_{dimer})$^{-1}$ s^{-1})	$N_2 + N_2O$ rate $\times 10^3$ per isolated Cu^{2+} (mol (mol Cu_i)$^{-1}$ s^{-1})
Cu(0.12)	0.56	1.23	1.05
Cu(0.36)	3.98	7.10	9.05
Cu(0.38)	4.71	7.84	11.80
Cu(0.58)	6.42	9.18	21.40
Cu(0.60)	6.64	8.52	30.20

Conclusions

H_2-TPR monitored by mass spectrometry and *in situ* X-ray absorption spectroscopy showed that the Cu on Cu–ZSM5 occurs predominantly as isolated exchanged Cu^{2+} and as exchanged Cu dimers, $\{Cu^{2+}–O^{2-}–Cu^{2+}\}^{2+}$ after calcination. These experiments did not detect bulk copper oxide (CuO), as also expected from the low pH in solution during synthesis and the limited extent to which it was possible to introduce Cu into the ZSM5 samples. Based on the amount of CO_2 that formed during CO-TPR, the fraction of the total Cu that appears in Cu dimers increased from 0.46 to 0.78 as Cu/Al ratios increased from 0.12 to 0.60. The Cu_{dimer}/Al ratio increased from 0.06 to 0.47, whereas the Cu^{2+}/Al ratio leveled off at ~0.15, suggesting that only a fraction of the Al-sites are sufficiently close to another Al-site for them to bind a Cu^{2+}. At higher Cu/Al ratios the average Cu–Cu distance decreases, and this allows a larger fraction of the Cu to form Cu–O–Cu bridges as observed from the increase in Cu dimers with increasing Cu/Al ratio. The Cu_{dimer}/Al and Cu^{2+}/Al ratios obtained from the amount of CO_2 formed in the CO-TPR are consistent with the amount of H_2O formed during H_2-TPR, and the amount of CO adsorbed after CO-TPR, and also with previously reported theoretical Al–Al distribution calculations.

The number of oxygen atoms removed as O_2 was significant smaller than that removed with H_2 or CO suggesting that only proximate Cu dimers autoreduce *via* recombinative desorption steps during O_2-TPD experiments. The fraction of the adsorbed oxygen atoms that can desorb from Cu dimers increased from 0.35 to 0.57 with increasing Cu/Al ratio, showing that a significant fraction of the Cu dimers remain isolated even at high Cu/Al ratios. Multiple peaks appear in both the O_2-TPD and the CO-TPR profiles indicating that Cu dimers exist in various geometries with different stability and reactivity towards O_2 and CO_2 formation.

The NO decomposition rate per Cu was found to increase with increasing Cu/Al ratio. This increase in rate occurred in parallel with increasing Cu_{dimer}/Al ratios and this correlation suggests that Cu dimers are the active sites for NO decomposition on Cu–ZSM5. The lower NO decomposition turnover rates (per Cu dimer) measured on the Cu–ZSM5 with lowest Cu content appears to reflect the higher oxygen stability on the Cu dimers first formed during ion exchange, as evidenced by the higher temperature required to form O_2 during O_2-TPD and CO_2 during CO-TPR experiments. Thus, the equilibrium between oxidized and reduced Cu dimers during NO decomposition is shifted towards oxidized Cu dimers; as a result, NO decomposition rates do not decrease as the temperature increases above 773 K, in contrast with the behavior observed on samples with higher Cu/Al ratio.

During synthesis, isolated Cu^{2+} and stable Cu dimers form initially at lower Cu/Al ratios, whereas unstable Cu dimers form when more Cu is exchanged into the catalyst. These unstable Cu dimers are responsible for the higher NO decomposition activity observed at higher Cu/Al ratios.

Acknowledgements

Patrick Da Costa acknowledges the financial support from the French Foreign Affairs Ministry in the form of a "Programme Lavoisier" Grant. The financial support for Björn Modén in the form of a grant from CF Miljöfonden and of Deuk Ki Lee from the Korea Science and Engineering Foundation (KOSEF) are also gratefully acknowledged. Portions of this research were carried out at the Stanford Synchrotron Radiation Laboratory, a national user facility operated by Stanford University on behalf of the U.S. Department of Energy, Office of Basic Energy Sciences.

References

1 M. Iwamoto, S. Yokoo, K. Sakai and S. Kawaga, *J. Chem. Soc., Faraday Trans.*, 1981, **177**, 1629.
2 M. Shelef, K. Otto and H. Gandhi, *Atmos. Environ.*, 1969, **3**, 107.
3 A. Amirnazmi and M. Boudart, *J. Catal.*, 1975, **39**, 383.
4 M. Iwamoto, H. Yahiro, W. Mizuno, W.-X. Zhang, Y. Mine, H. Furukawa and S. Kagawa, *J. Phys. Chem.*, 1992, **96**, 9360.
5 S. C. Larsen, A. W. Aylor, A. T. Bell and J. A. Reimer, *J. Phys. Chem.*, 1994, **98**, 11 533.
6 E. Giamello, D. Murphy, G. Magnacca, C. Morterra, Y. Shioya, T. Nomura and M. Anpo, *J. Catal.*, 1992, **136**, 510.
7 Y. Li and W. K. Hall, *J. Catal.*, 1991, **129**, 202.
8 H.-J. Jang, W. K. Hall and J. L. d'Itri, *J. Phys. Chem.*, 1996, **100**, 9416.
9 W. Grunert, N. W. Hayes, R. W. Joyner, E. S. Shpiro, M. R. H. Siddiqui and G. N. Baeva, *J. Phys. Chem.*, 1994, **98**, 10 832.
10 D.-J. Liu and H. J. Robota, *Catal. Lett.*, 1993, **21**, 291.
11 D.-J. Liu and H. J. Robota, *Appl. Catal., B*, 1993, **4**, 155.
12 M. Shelef, *Catal. Lett.*, 1992, **15**, 305.
13 A. W. Aylor, S. C. Larsen, J. A. Reimer and A. T. Bell, *J. Catal.*, 1995, **157**, 592.
14 G. Spoto, A. Zecchina, S. Bordiga, G. Ricchiardi and G. Martra, *Appl. Catal., B*, 1994, **3**, 151.
15 W. K. Hall and J. Valyon, *Catal. Lett.*, 1992, **15**, 311.
16 J. Valyon and W. K. Hall, *J. Phys. Chem.*, 1993, **97**, 1204.
17 J. Valyon and W. K. Hall, *J. Catal.*, 1993, **143**, 520.
18 J. Sarkany, J. L. d'Itri and W. M. H. Sachtler, *Catal. Lett.*, 1992, **16**, 241.
19 G. D. Lei, B. J. Adelman, J. Sarkany and W. M. H. Sachtler, *Appl. Catal., B.*, 1995, **5**, 245.
20 T. Beutel, J. Sarkany, G. D. Lei, J. Y. Yan and W. M. H. Sachtler, *J. Phys. Chem.*, 1996, **100**, 845.
21 G. Moretti, *Catal. Lett.*, 1994, **23**, 135.
22 B. Moden, P. Da Costa, B. Fonfe, D. K. Lee and E. Iglesia, *J. Catal.*, 2002, **209**, 75.
23 B. Moden, P. Da Costa, D. K. Lee and E. Iglesia, *J. Phys. Chem B*, 2002, in press.
24 G. D. Meitzner and E. Iglesia, *Catal. Today*, 1999, **53**, 433.
25 D. G. Barton, S. L. Soled, G. D. Meitzner, G. A. Fuentes and E. Iglesia, *J. Catal.*, 1999, **181**, 57.
26 T. Ressler, http://ourworld.compuserve.com/homepages/t_ressler/.
27 (*a*) T. Ressler, *J. Phys. IV*, 1997, **7**, C2; (*b*) T. Ressler, *J. Synchrotron Radiat.*, 1998, **5**, 118.
28 E. R. Malinowski and D. G. Howery in *Factor Analysis in Chemistry*, Wiley, New York, 1981.
29 G. D. Meitzner and E. S. Huang, *Fresenius' J. Anal. Chem.*, 1992, **342**, 61.
30 J. Dedecek and B. Wichterlova, *J. Phys. Chem. B*, 1997, **101**, 10 233.

31 Y. Zhang, K. M. Lee, A. F. Sarofim, Z. Hu and M. Flytzani-Stephanopoulos, *Catal. Lett.*, 1995, **31**, 75.
32 M. Iwamoto, H. Yahiro, K. Tanda, N. Mizuno and Y. Mine, *J. Phys. Chem.*, 1991, **95**, 3727.
33 A. V. Kucherov, A. A. Slinkin, D. A. Kondratev, T. N. Bondarenko, A. M. Rubinstein and K. M. Minachev, *Zeolites*, 1985, **5**, 320.
34 C. Lamberti, S. Bordiga, M. Salvalaggio, G. Spoto, A. Zecchina, F. Geobaldo, G. Vlaic and M. Bellatreccia, *J. Phys. Chem. B.*, 1997, **101**, 344.
35 K. C. C. Kharas, D.-J. Liu and H. J. Robota, *Catal. Today*, 1995, **26**, 129.
36 J. M. Tranquada, S. M. Heald and A. R. Moodenbaugh, *Phys. Rev. B*, 1987, **36**, 5263.
37 J. M. Brown, L. Powers, B. Kincaid, J. A. Larrabee and T. G. Shirp, *J. Am. Chem. Soc.*, 1980, **102**, 4210.
38 L. S. Kau, D. J. Spira-Salomon, J. E. Penner-Hahn, K. O. Hodgson and E. I. Salomon, *J. Am. Chem. Soc.*, 1987, **109**, 6433.
39 Y. Kuroda, Y. Yoshikawa, S. Konno, H. Hamano, H. Maeda, R. Kamashiro and M. Nagao, *J. Phys. Chem.*, 1995, **99**, 10 621.
40 J. Sarkany and W. M. H. Sachtler, *Zeolites*, 1994, **14**, 7.
41 M. J. Rice, A. K. Chakraborty and A. T. Bell, *J. Catal.*, 1999, **186**, 222.
42 M. J. Rice, A. K. Chakraborty and A. T. Bell, *J. Catal.*, 2000, **194**, 278.
43 M. J. Rice, A. K. Chakraborty and A. T. Bell, *J. Phys. Chem. B*, 2000, **104**, 9987.
44 E. Eranen, N. Kumar and L.-E. Lindfors, *Appl. Catal. B.*, 1994, **4**, 213.
45 Y. Teraoka, C. Tai, H. Ogawa, H. Furukawa and S. Kagawa, *Appl. Catal. A*, 2000, **200**, 167.
46 Z. Wang, A. V. Sklyarov and G. W. Keulks, *Catal. Today*, 1997, **33**, 291.
47 M. Iwamoto, H. Furukawa, Y. Mine, F. Uemura, S. Mikuriya and S. Kagawa, *J. Chem. Soc., Chem. Commun.*, 1986, 1272.